JOURNAL OF MATERIALS SCIENCE 18 (1983) 1365–1373

Bending properties of creased zones of paperboard related to interlaminar defects

LEIF CARLSSON*, ALF DE RUVO, CHRISTER FELLERS
Swedish Forest Products Research Laboratory, Department of Paper Technology, Drottning Kristinas Väg 55, S-114 86 Stockholm, Sweden

A parallel beam model is presented for the bending behaviour of locally delaminated zones (creased zones) of paperboard. It is shown that the bending moment and the force levels are strongly dependent on the geometry and elastic properties of the creased zone. A favourable condition for low crease stiffness is a large number of long interlaminar failures. Experimental measurements of the crease stiffness and maximum bending moment for paperboards with implanted defects of various lengths and numbers were in reasonably good agreement with the crease stiffness predicted by the parallel beam model.

1. Introduction

Paperboard is an unique material with regard to its performance in packaging operations since it is easily converted from a rigid material to a flexible one in the creasing operation where the aim is to achieve a local reduction in the bending stiffness and maximum bending moment. In this way flat blanks are easily transformed to boxes by the introduction of "hinges" along predetermined lines.

Fig. 1 presents a scheme of the creasing operation. In this operation the paperboard is forced into the recessed areas by means of a male rule (Figs. 1a and b), and the combined action of bending and shear causes deformation and interlaminar failure of the board so that a creased zone is obtained (Fig. 1c). Thus the creasing operation preconditions the paperboard so that a hinge is introduced which facilitates bending (Fig. 1d).

Although the creasibility of paperboard is a problem of significant technological importance it does not appear to have received much attention from the materials science point of view.

Emslie and Brenneman [1] reported some important properties of paperboard for obtaining good creasability, but no rigorous analysis of the bending of a creased zone was presented. More recently Carlsson *et al.* [2] investigated the interlaminar stresses and the tendency for propagation of an interlaminar crack in the creased zone by the finite element method.

It is to be expected that the bending properties of the creased zone, such as crease stiffness and maximum bending moment, are strongly dependent on the extent of delamination. This paper is concerned with the bending behaviour of paperboard with implanted interlaminar defects with different geometries and of different numbers. In the analysis of the delaminated board the delamined zone is modelled as two beams in parallel, one transmitting tensile forces and one transmitting compressive forces.

2. Bending analysis formulation

Even if the creased zone consists of several delaminated layers, cf. Fig. 1, it is in this analysis, modelled by two equivalent beams in parallel, according to Fig. 2, that Beam 1 transmits a tensile force while beam 2 transmits a compressive force in the buckled state. The bending angle is denoted by ϕ, the distance between the centres of the beams by h, the bending moment by M_0 and the length of the beams by $2L$.

Consider the portion of beam 1 located to the right of the vertical symmetry line in Fig. 2. With the coordination axes as shown in Fig. 3 the

*Present address: The Aeronautical Research Institute of Sweden, S-161 11 Bromma, Sweden.

0022–2461/83 $03.00 + .12

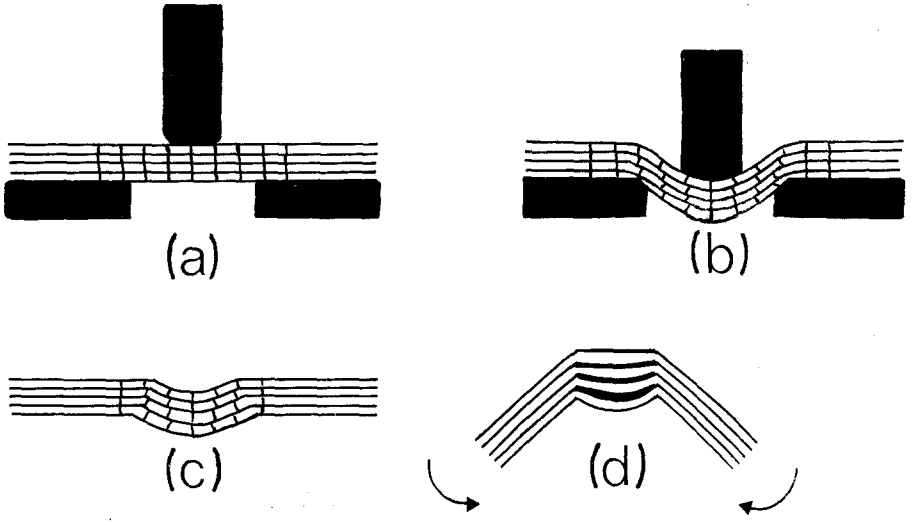

Figure 1 Schematic view of the creasing and bending operations. (a) and (b) The board is deformed by the action of a male rule. (c) Appearance of the creased zone. (d) Bending of the creased zone.

differential equation for the deflection curve is [3]

$$EI_1 \frac{d\theta_1}{ds} = -P\,[y(L) - y(s)] + M_1 \qquad (1)$$

where E is the elastic modulus of the material, I_1 is the moment of inertia of beam 1, θ_1 is the angle between the horizontal and the tangent to the deflection curve of beam 1, s is the length of the deflection curve measured from the vertical symmetry line in Fig. 2, P is the axial force and M_1 is the bending moment at the right-hand boundary of beam 1. Since

$$\frac{dy}{ds} = \sin\theta_1 \qquad (2)$$

we obtain

$$y(L) - y(s) = -\int_L^s \sin\theta_1 \, ds'. \qquad (3)$$

After substitution in Equation 1 and differentiation with respect to θ_1

$$EI_1 \frac{d^2\theta_1}{ds^2} - P\sin\theta_1 = 0. \qquad (4)$$

In an analogous manner, the differential equation for the deflection curve of beam 2 may be shown to be:

$$EI_2 \frac{d^2\theta_2}{ds^2} + P\sin\theta_2 = 0 \qquad (5)$$

with the symbols I_2 and θ_2 for beam 2 defined in the same way as the corresponding symbols for beam 1.

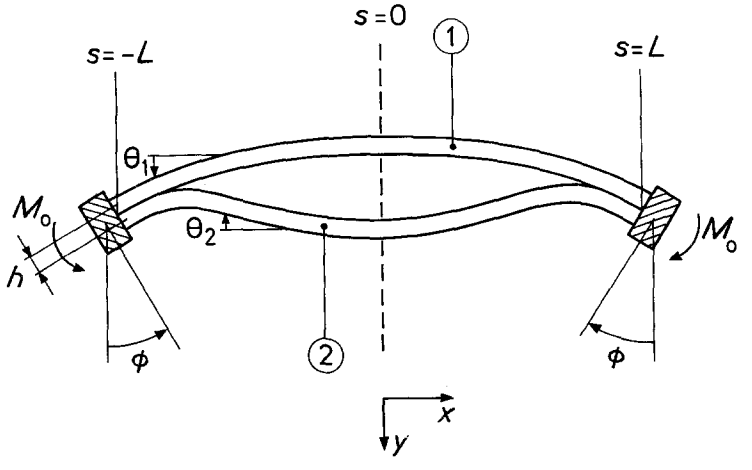

Figure 2 Parallel beam model of the creased zone.

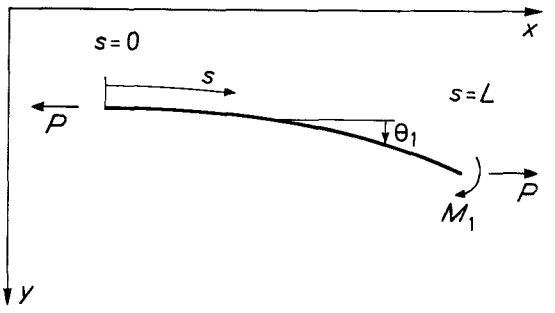

Figure 3 Coordinates used to express the deflection curve of beam 1 when subjected to axial force and bending moment.

The following boundary conditions apply

$$\theta_1(L) = \theta_2(L) = \phi \tag{6}$$

$$\theta_1(0) = \theta_2(0) = 0. \tag{7}$$

Bending of the parallel beam configuration is caused by a rotation (ϕ) of the ends, see Fig. 2. The following boundary condition for the horizontal displacements at the right-hand boundary can then be formulated from geometrical considerations:

$$x_1(L) - x_2(L) = h \sin\phi \tag{8}$$

where $x_1(L)$ and $x_2(L)$ are the horizontal displacements of the deflection curves at the right-hand boundaries of beams 1 and 2, respectively.

Since $dx/ds = \cos\theta$, Equation 8 can be written:

$$\int_0^L (\cos\theta_1 - \cos\theta_2)\, ds = h \sin\phi. \tag{9}$$

These equations enable θ_1 and θ_2 to be determined as a function of s. Finally, the bending moment M_0 is obtained by

$$M_0 = EI_1 \left(\frac{d\theta_1}{ds}\right)_{s=L} + EI_2 \left(\frac{d\theta_2}{ds}\right)_{s=L} + Ph \cos\phi. \tag{10}$$

An approximate solution to the above equations is presented in the Appendix.

2.1. Influence of geometry

The influence of the geometry of the creased zone on the bending moment and the forces in the beams can be studied by the parallel beam model presented above. Dimensionless quantities, derived from the equations in the appendix, are used. The parameters used to characterize the geometry of the creased zone are h/L and the moment of inertia ratio I_2/I_1. Both I_1 and I_2 are very sensitive to the extent of delamination in the creased zone because the moment of inertia of a beam is proportional to the cube of its thickness. For example, if instead of a homogeneous beam, beam 2 represents two beams of half the thickness, I_2 will be reduced by a factor four since the two beams are uncoupled.

Fig. 4 shows the dimensionless bending moment

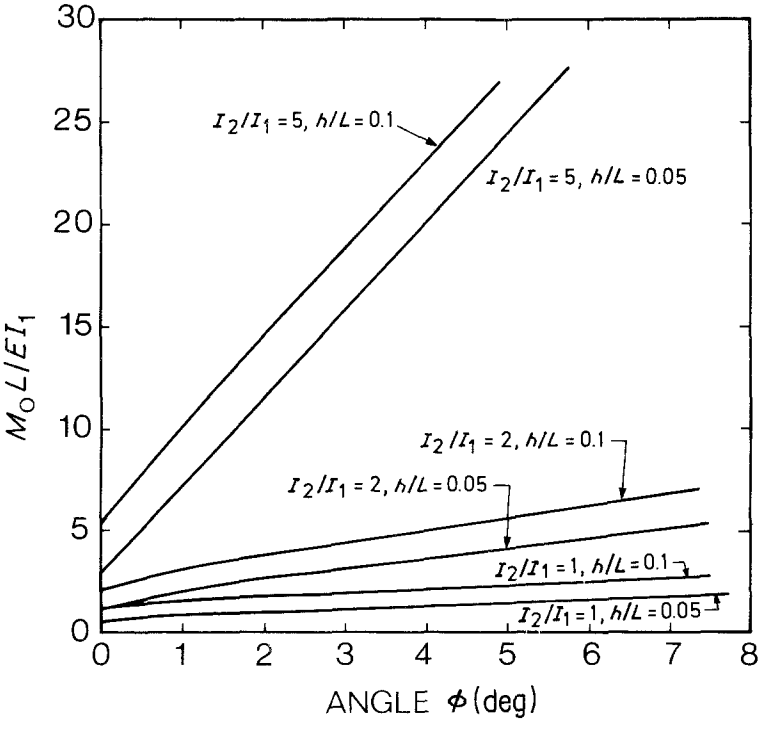

Figure 4 Theoretical dimensionless bending moment against bending angle.

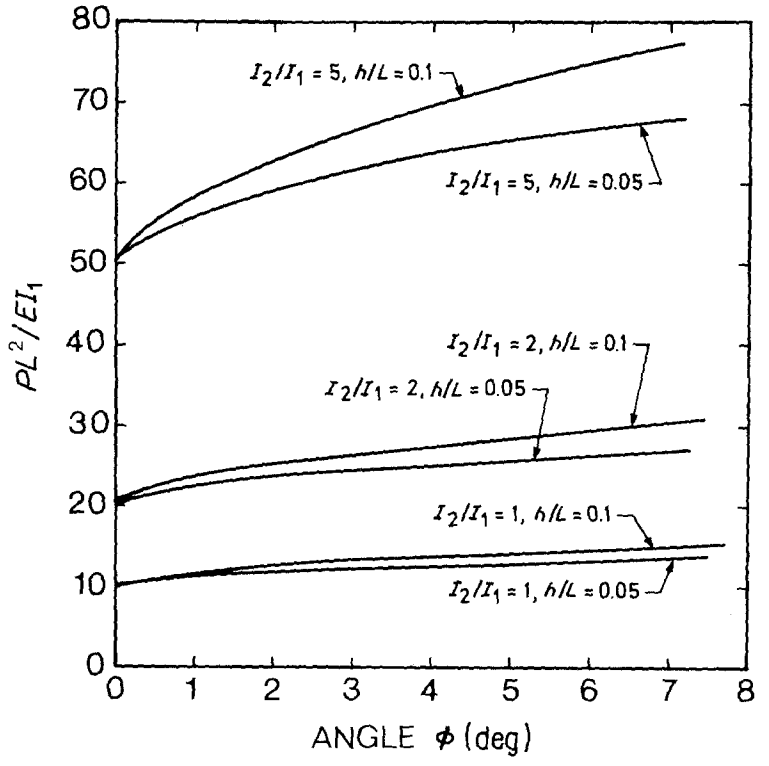

Figure 5 Theoretical dimensionless force against bending angle.

M_0L/EI_1 against the bending angle. It is noted that the bending moment is greater than zero for a zero bending angle. This is so because the model permits no bending before the critical buckling load of beam 2 is reached.

It is clear that the bending moment is highly sensitive to the moment of inertia ratio. A reduction in I_2 with all other parameters constant obviously leads to a large reduction in the bending moment. The value of h/L does not influence the dimensionless bending moment appreciably. However, an increase in length of the delaminated zone ($2L$) leads, with all other parameters constant, to a reduction in the absolute bending moment.

Fig. 5 shows the dimensionless force PL^2/EI_1 against the bending angle. As in the case of the bending moment, the dimensionless force is rather insensitive to the h/L ratio while the absolute force decreases with decreasing I_2/I_1 ratio and increasing length ($2L$).

3. Experimental details

In order to vary the geometry and the extent of delamination of the creased zone in a controlled way, defects consisting of strips of 0.01 mm thick aluminium foils were implanted between the plies in an eight-ply paperboard in a manner exemplified in Fig. 6. The paperboard was made from bleached chemical pulp in a laboratory Formette Dynamique sheet former and the strips were introduced during the sheet forming process.

The defect strips were in some cases 2 mm and in other cases 3 mm in width and they were aligned either with the lowest modulus direction (CD) or with the highest modulus direction

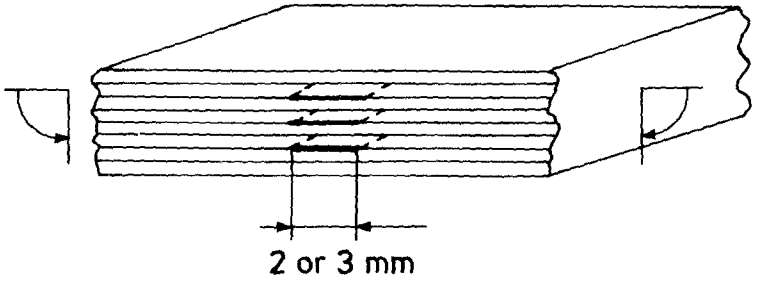

Figure 6 Example showing how interlaminar defects are implanted at interfaces 2, 4 and 6. The debonded length is 2 or 3 mm.

TABLE I Location and length of implanted interlaminar defects. Note that interface 1 is located between ply 1 (top ply) and ply 2 in the eight-ply construction

Number of defects	Length (mm)	Sample identification	Interface						
			1	2	3	4	5	6	7
1	2	1/2						x	
3	2	3/2		x		x		x	
3	3	3/3		x		x		x	
7	2	7/2	x	x	x	x	x	x	x
7	3	7/3	x	x	x	x	x	x	x

(MD). 1, 3 and 7 defects were implanted at different locations according to Table I.

A paperboard was also made with no implanted defects in order to permit an evaluation of the material properties. The thickness [4], grammage (weight per unit area), density and the uniaxial stress–strain properties evaluated using a standard Instron testing machine are presented in Table II.

Earlier studies [1, 2] show that the form of the creased zone and consequently the geometry of the tools used in the creasing operation plays an important role for the behaviour in the bending operation. The geometry used in the creasing operation was, therefore, the same for all samples. The creasing operation was performed with a PATRA Carton Board Creaser [5] developed for laboratory testing of the creasability of paperboard. The groove width was 2.3 mm, the width of the rule 0.7 mm and the vertical displacement of the paperboard at the centre of the creasing zone was 0.3 mm, cf. Fig. 1.

The bending properties of the creased samples, namely crease stiffness and bending strength, were evaluated in a device developed for measuring the pure bending properties of the paper [6]. With this device the sample is clamped in two rotatable clamps and subjected to a pure bending moment. The crease stiffness of the creased samples was evaluated from the initial slope of the bending moment against the bending angle curve ($\Delta M_0/\Delta\phi$) and the bending strength from the maximum bending moment. In order to minimize the influence on crease stiffness of the uncreased portion of the samples, a short free span of 5 mm was used in all cases.

For the determination of the geometrical parameters h/L and I_2/I_1 scanning electron microscope (SEM) pictures were taken of samples which were kept in the bent state by gluing one edge of the sample to a piece of paper.

4. Results and discussion

4.1. Fractography

Figs. 7 to 9 show representative scanning electron micrographs of the creased zone of sample 0/0 MD, 3/3 MD and 7/3 MD, respectively, bent to both small and large angles. Fig. 7 shows that a major interlaminar crack exists at small bending angles in a sample without implanted defects (0/0 MD). At larger angles a significantly greater extent of delamination is noted. This is likely to be due to propagation of incipient interply failure at higher stress levels, see [2].

Fig. 8 shows a sample with three implanted defects (3/3 MD). At larger angles failure is apparent at the lower part of the right-hand boundary of the creased zone indicating a region of high compressive stresses. Fig. 9 shows the appearance of a creased zone of a sample with seven implanted defects (7/3 MD).

4.2. Determination of the parameters used in the theory

It appears from Figs. 7 to 9 that only the outermost ply is subjected to tension and all others to compression. This means that if the creased zone is divided up into N beams by the implanted defects, one beam is subjected to tension and $N-1$ beams to compression, i.e.

TABLE II Properties of paperboard with no implanted defects. t = thickness, w = grammage, ρ = density, E = elastic modulus, σ_t = ultimate tensile stress and ϵ_t = failure strain

Direction	t (mm)	w (g m^{-2})	ρ (kg m^{-3})	E (MN m^{-2})	σ_t (MN m^{-2})	ϵ_t (%)
MD	0.47	425	910	9700	98.0	2.8
CD				5740	73.0	4.0

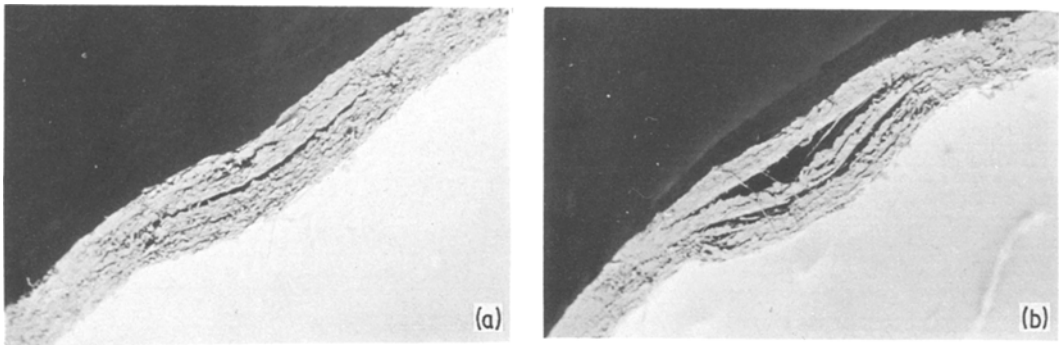

Figure 7 Creased paperboard with no implanted defects (0/0 MD) bent through (a) a small and (b) a large angle.

$$I_1 = t_1^3/12 \quad (11)$$

where t_1 is the thickness of the beam under tension.

Since the beams under compression are uncoupled,

$$I_2 = (N-1)(t_k)^3/12 \quad (12)$$

where t_k is the thickness of each compressed beam.

In order to be able to compare theory with experiment, the parameters h/L and I_2/I_1 were determined from the SEM pictures of the creased samples with implanted defects. The parameters h and L were measured according to Fig. 10. EI values were obtained from the material properties in Table II and the number of delaminated plies according to Equations 11 and 12. The parameters obtained are tabulated in Table III. Note the very wide range of I_2/I_1 and EI_1 values.

4.3. Bending properties

The bending moment was recorded as a function of bending angle for both uncreased and creased samples. Table IV gives the measured values of crease stiffness and bending strength.

A comparison of the crease stiffness of boards with only one defect implanted with that of the boards with no defects implanted show no noticeable reduction in crease stiffness. However, the presence of more defects reduces the crease stiffness to a great extent. The greatest reduction in crease stiffness is obtained for the board with the most and the longest defects which is in qualitative agreement with the theory.

The bending strength is also reduced to a great extent by the presence of implanted defects, especially if comparison is made with the data for the uncreased paperboard.

4.4. Theory versus experiment

The parameters h/L and I_2/I_1 obtained from Table III were inserted in Equations 4, 5, 9 and 10 and the dimensionless bending moment against the bending angle curves, such as those shown in Fig. 4, were plotted. As pointed out earlier, since the bending of creased zone is a post-buckling problem the theoretical crease stiffness ($\Delta M_0/\Delta\phi$) is defined as the slope of the bending moment against the bending angle. Since the dimensionless moment is an almost linear function of the angle, the

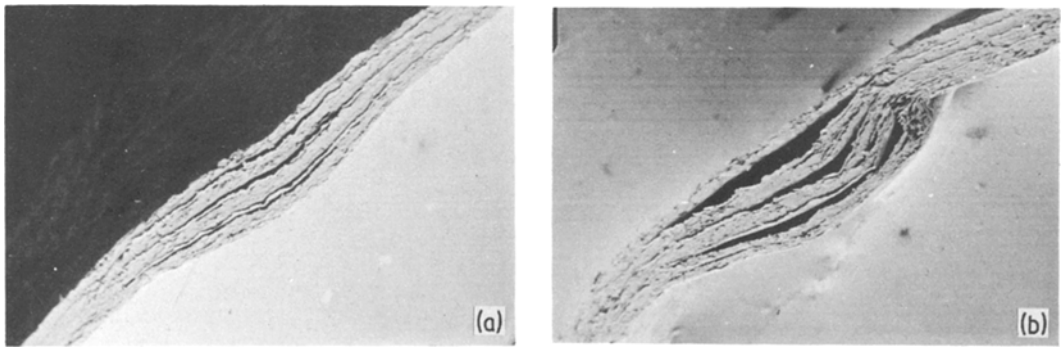

Figure 8 Creased paperboard with three defects (3/3 MD) bent through (a) a small and (b) a large angle.

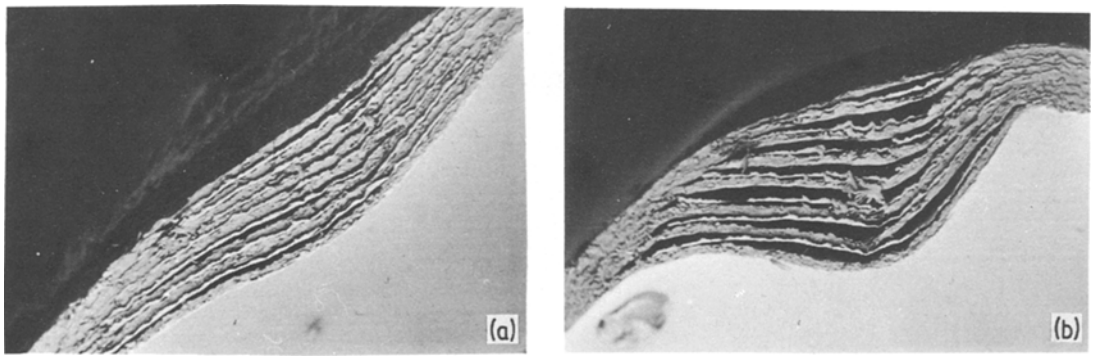

Figure 9 Creased paperboard with seven defects, i.e. at all ply interfaces, (7/3 MD) bent through (a) a small and (b) large angle.

average slope in the interval 0 to 10° was evaluated from the curves.

The following theoretical dimensionless crease stiffness was thus obtained:

$$S_T = \Delta (M_0 L/EI_1)/\Delta\phi. \quad (13)$$

The experimental crease stiffness ($\Delta M_0/\Delta\phi$) values given in Table IV, scaled with respect to L and EI_1 given in Table III, give the experimental dimensionless crease stiffness:

$$S_E = \Delta M_0 \, [L/(\Delta\phi \times EI_1)]. \quad (14)$$

Fig. 11 shows theoretical and experimental values of the dimensionless crease stiffness plotted on a logarithmic scale against the number of defects. Note that the difference between MD and CD is very small and that the defect size has a small influence compared with that of the number of defects.

The experimental crease stiffness values are very close to the theoretical values for the samples with one defect tested in both principal material directions. For the samples with 3 and 7 defects, the theoretical crease stiffness values are higher than those experimentally observed.

Since the crease stiffness is very sensitive to the properties of the constituent plies in the creased zone and to the fixity of the ends of the beams, the low crease stiffness values observed are likely to be due to damage to the plies caused in the creasing operation. It is probable that the boards with many thin plies are more sensitive to the action of the creasing tools than the boards with only one implanted defect.

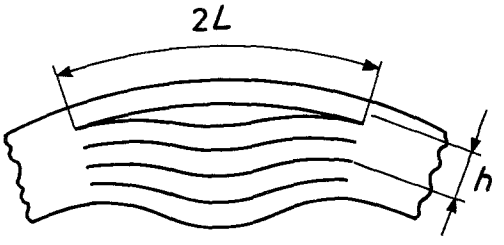

Figure 10 The parameters h and L of the creased zone.

5. Conclusions

The crease stiffness and the bending strength of creased zones with interlaminar defects were found to decrease strongly with the number of interlaminar defects.

The bending of the creased delaminated zones was analysed by a parallel beam configuration. An approximate solution of the equations for the deflection curve enables the bending moment to be obtained in the elastic region as a function of the bending angle.

Experimental dimensionless crease stiffness values showed an overall good agreement with predicted values. Observed deviations are attributed to damage to the plies in the creased zone during the creasing operation.

In practice it is necessary to create hinge-like performance zones in paperboard. This study shows the importance of the fractography to

TABLE III Parameters evaluated from SEM pictures of the creased zone

Sample	h (mm)	L (mm)	I_2/I_1	EI_1 (mNm)
1/2 MD	0.24	1.3	0.037	37.7
1/2 CD	0.24	1.1	0.037	22.3
3/2 MD	0.24	1.2	3	1.40
3/3 MD	0.23	1.8	3	1.23
7/2 MD	0.24	1.2	7	0.175
7/3 MD	0.23	1.7	7	0.154

TABLE IV Bending properties evaluated for uncreased and creased samples. MD = longitudinal direction, CD = transverse direction

Sample	Crease stiffness (mNm/m°)	Bending strength (Nm m^{-1})
Uncreased MD	–	2.08
Uncreased CD	–	1.61
0/0* MD	262	1.16
0/0 CD	182	0.93
1/2 MD	258	1.28
1/2 CD	185	0.99
3/2 MD	209	1.24
3/3 MD	181	1.13
7/2 MD	162	0.95
7/3 MD	152	0.83

*Sample 0/0 is a creased sample with no implanted defects.

regulate this behaviour. The character of the interlaminar failure is, of course, strongly related to the structure of the paperboard. Any means of increasing the extent of delamination in the creased zone, such as a suitable disposition of raw material in a multi-ply board, will consequently improve the creasability of the material.

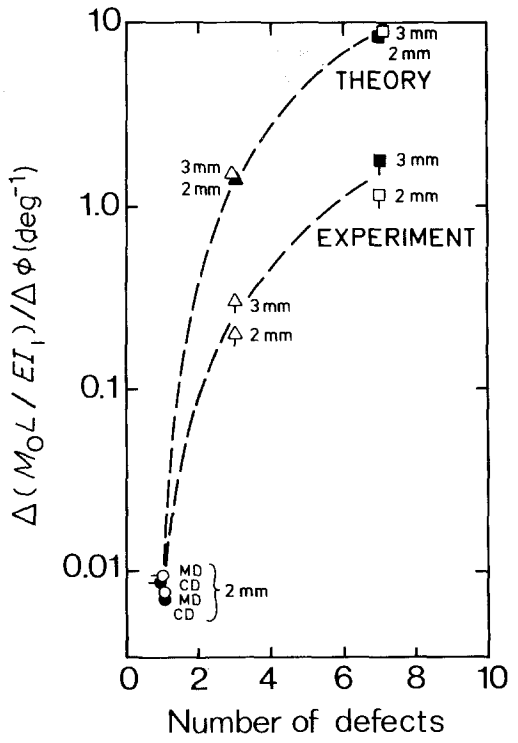

Figure 11 Theoretical and experimental values of the dimensionless crease stiffness.

Acknowledgement

Part of this work was performed by one of the authors, L. Carlsson, as a partial requirement for the achievement of a MSc degree. He is grateful for valuable advice form Dr S. Herlitz and Professor H. C. Fischer of Uppsala University.

The authors wish to thank Ms B. Möllerberg for skilful experimental assistance and Dr E. Treiber for the preparation of the scanning electron micrographs.

Appendix

Equations 4 to 9 used to calculate the deflection curve of the parallel beam configuration may be summarized as:

$$EI_1\theta_1'' - P\sin\theta_1 = 0 \quad \text{(A1)}$$

$$EI_2\theta_2'' + P\sin\theta_2 = 0 \quad \text{(A2)}$$

with the boundary conditions:

$$\theta_1(L) = \theta_2(L) = \phi \quad \text{(A3)}$$

$$\theta_1(0) = \theta_2(0) = 0 \quad \text{(A4)}$$

$$\int_0^L (\cos\theta_1 - \cos\theta_2)\,ds = h\sin\phi. \quad \text{(A5)}$$

To permit an analytical solution to the above equations, the $\sin\theta$ and $\cos\theta$ terms are replaced by a few terms in their respective Taylor series.

Equation A2 is used to determine post-buckling behaviour of the beam in compression. Therefore a third-order term is included in the Taylor series approximation to obtain a better approximation to the problem. In the other equations, only first or second order terms are included.

With $\gamma_1^2 = PL^2/EI_1$ and $\gamma_2^2 = PL^2/EI_2$ we thus obtain:

$$\theta_1'' - \frac{\gamma_1^2}{L^2}\theta_1 = 0 \quad \text{(A6)}$$

$$\theta_2'' + \frac{\gamma_2^2}{L^2}\left(\theta_2 - \frac{\theta_2^3}{6}\right) = 0 \quad \text{(A7)}$$

$$\tfrac{1}{2}\int_0^L (\theta_2^2 - \theta_1^2)\,ds = h\phi. \quad \text{(A8)}$$

Equation A6 has the solution

$$\theta_1 = \phi\sin h\,(\gamma_1 s/L)/\sin h\,\gamma_1. \quad \text{(A9)}$$

The solution of Equation A7 may be obtained by a Fourier series [7]. To a first approximation we obtain

$$\theta_2 = A_1 \sin \xi s + A_3 \sin 3\xi s \qquad \text{(A10)}$$

where $|A_3| \ll |A_1|$.

Substituting Equation A10 in Equation A7, we obtain after some algebraic manipulation

$$\xi \simeq (\gamma_2/L)\,[1-(A_1^2/8)]^{1/2} \qquad \text{(A11)}$$

$$A_3 = \frac{-A_1}{[(192/A_1^2)-21]} \qquad \text{(A12)}$$

Substitution of Equations A9 and A10 in Equation A8 yields

$$\frac{\phi^2}{4 \sin h^2 \gamma_1}\left[1-\frac{\sin h\, 2\gamma_1}{2\gamma_1}\right] + \left(\frac{A_1}{2}\right)^2\left[1-\frac{\sin 2\gamma_2\beta}{2\gamma_2\beta}\right] + A_1A_3 \times \left[\frac{\sin 2\gamma_2\beta}{4\gamma_2\beta}-\frac{\sin 4\gamma_2\beta}{8\gamma_2\beta}\right] = \left(\frac{h}{L}\right)\phi \qquad \text{(A13)}$$

in which $\beta = [1-(A_1^2/8)]^{1/2}$.

The boundary condition Equation A3 gives in Equation A10

$$A_1\left[\sin(\gamma_2\beta)-\frac{\sin(3\gamma_2\beta)}{(192/A_1^2)-21}\right] = \phi \qquad \text{(A14)}$$

The force P in the beams is expressed by the dimensionless parameters γ_1 and γ_2 where

$$\gamma_1 = \gamma_2 (I_2/I_1)^{1/2} \qquad \text{(A15)}$$

For a given geometry (h/L and I_2/I_1) and value of γ_2, Equations A13 and A14 may be combined to give A_1 and thus ϕ by means of an iterative procedure.

References

1. A. G. EMSLIE and R. S. BRENNEMAN, *Tappi* **50** (1967) 289.
2. L. CARLSSON, C. FELLERS, B. WESTERLIND and J. BÄCKLUND, *Svensk Papperstidn.* **85** (1982) R121.
3. S. TIMOSHENKO, "Theory of Elastic Stability" (McGraw Hill, New York, 1936).
4. H. HOLLMARK, C. FELLERS and B. NORMAN, "Definition and measurement of density" in "Paper Structure and Paper Properties", edited by J. A. Bristow (Marcel Dekker, New York) in press.
5. "The Patra Carton Board Creaser", Printing, Packaging and Allied Trades Research Association, Patra House, Randalls Road, Leatherhead, Surrey, England.
6. C. FELLERS and L. CARLSSON, *Tappi* **62** (1979) 107.
7. N. W. McLACHAN, "Ordinary Non-linear Differential Equations in Engineering and Physical Sciences" (Claredon press, Oxford, 1950).

Received 14 May
and accepted 4 October 1982